# Direct simulation of evolution and control of three-dimensional instabilities in attachment-line boundary layers

## By RONALD D. JOSLIN

Fluid Mechanics and Acoustics Division, Mail Stop 170, NASA Langley Research Center, Hampton, Virginia 23681-0001, USA

The spatial evolution of three-dimensional disturbances in an attachment-line boundary layer is computed by direct numerical simulation of the unsteady, incompressible Navier–Stokes equations. Disturbances are introduced into the boundary layer by harmonic sources that involve unsteady suction and blowing through the wall. Various harmonic-source generators are implemented on or near the attachment line, and the disturbance evolutions are compared. Previous two-dimensional simulation results and nonparallel theory are compared with the present results. The three-dimensional simulation results for disturbances with quasi-two-dimensional features indicate growth rates of only a few percent larger than pure two-dimensional results; however, the results are close enough to enable the use of the more computationally efficient, two-dimensional approach. However, true three-dimensional disturbances are more likely in practice and are more stable than two-dimensional disturbances. Disturbances generated off (but near) the attachment line spread both away from and toward the attachment line as they evolve. The evolution pattern is comparable to wave packets in flat-plate boundary-layer flows. Suction stabilizes the quasi-two-dimensional attachment-line instabilities, and blowing destabilizes these instabilities; these results qualitatively agree with the theory. Furthermore, suction stabilizes the disturbances that develop off the attachment line. Clearly, disturbances that are generated near the attachment line can supply energy to attachment-line instabilities, but suction can be used to stabilize these instabilities.

## 1. Introduction

Many instability mechanisms can occur that cause the breakdown of laminar flow to turbulence on swept wings; however, this discussion will focus on those disturbances that evolve near the attachment-line region (near the leading edge). Turbulent contamination, which results from turbulence at a fuselage/wing juncture, can travel out over the wing and cause laminar flow on the wing to become turbulent. To prevent this contamination, devices such as the Gaster bump (1965) or suction (see Pfenninger 1977), implemented near the wing root, can halt the turbulent attachment-line boundary layer from sweeping out over the entire wing.

Although the problem of turbulent contamination can be avoided by using a mechanical device, a Reynolds number must exist beyond which disturbances that are generated by either surface imperfections or particulates on the wing, coupled
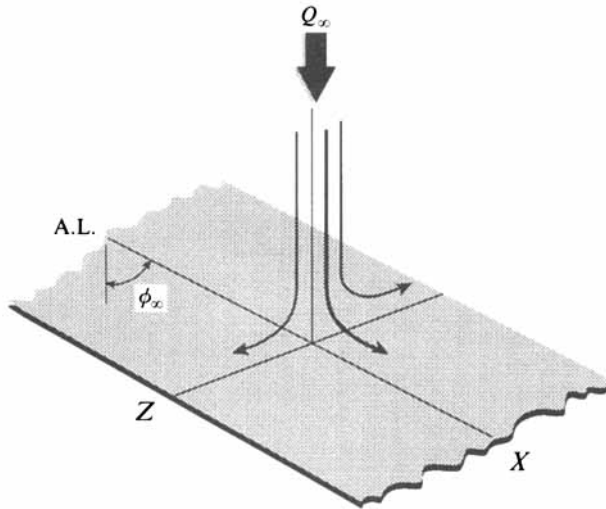
FIGURE 1. Sketch of attachment-line region of swept Hiemenz flow.

with noise, will eventually cause transition. Gaster (1967) first examined the small-amplitude disturbance problem by using acoustic excitation along the attachment line of a swept cylinder model. Gaster generated sine waves with various frequencies that were detected in the flow by a hot-film gauge on the attachment line. He noted that the recorded oscillations had preferred frequency bands that changed with tunnel speed and that this behaviour was reminiscent of travelling-wave instabilities. From his measurements, he concluded that the small-amplitude disturbances in an attachment-line boundary layer were stable for momentum-thickness Reynolds numbers $R_\theta$ below 170. Later, Cumpsty & Head (1969) experimentally studied large-amplitude disturbances and turbulent flow along the attachment line of a swept-wing model. Without artificially tripping the boundary-layer instabilities, they observed that laminar flow is stable to small-amplitude disturbances up to $R_\theta \approx 245$ (which corresponds to the top speed of the tunnel). At the same time, Pfenninger & Bacon (1969) used a wing swept to 45° to study the attachment-line instabilities in a wind tunnel capable of reaching speeds sufficient to obtain unstable disturbances. With hot wires, they observed regular sinusoidal oscillations with frequencies comparable to the most unstable two-dimensional modes of theory; these modes caused transition to occur at about $R_\theta \approx 240$. A continued interest in the transition initiated near the attachment line of swept wings led Poll (1979, 1980) to perform additional experiments with the swept circular model of Cumpsty & Head (1969). Like Pfenninger & Bacon (1969), Poll observed disturbances that amplified along the attachment line. He noted that no unstable modes were observed below $R_\theta = 230$.

With nonparallel stability theory, Hall, Malik & Poll (1984) studied the linear stability of the attachment-line boundary-layer flow called swept Hiemenz flow, which is shown in figure 1. This three-dimensional base flow is a similarity solution of the Navier–Stokes equations; hence, its use is advantageous in stability analyses. With a nonparallel theory, Hall *et al.* (1984) determined neutral curves with and without steady suction and blowing and demonstrated that the attachment-line boundary layer can theoretically be stabilized (destabilized) with small amounts of suction (blowing). Theofilis (1993a) performed a direct numerical simulation, based on Fourier-series assumptions, of the two-dimensional linear disturbances propagating
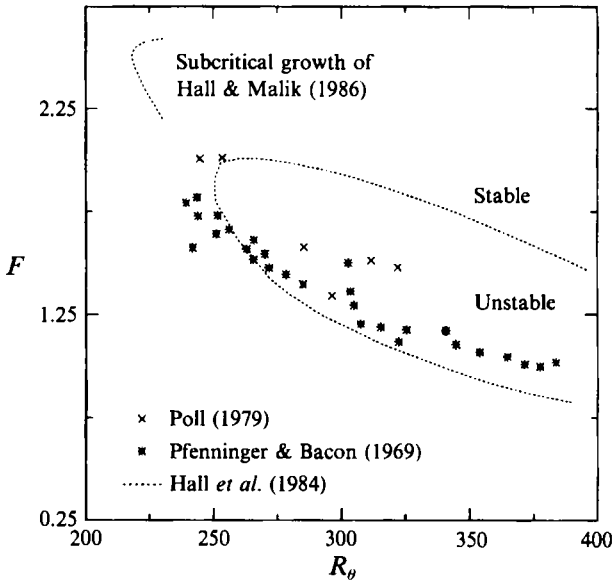
FIGURE 2. Neutral curve, experimental regions of instability growth, and theoretical region of subcritical growth in attachment-line boundary layer.

along the attachment line of swept Hiemenz flow. The direct numerical simulation results agreed with the nonparallel theory of Hall *et al.* (1984) near the upper branch of the neutral curve; however, the computations predicted growing modes in a region of theoretical decay near the lower branch. Theofilis (1993*a*) attributed the disagreement between computational and theoretical results near the lower branch of the neutral curve to the lack of direct numerical simulation grid resolution. The recent spatial direct numerical simulation results of Joslin (1994) for swept Hiemenz flow indicate good agreement (less than 2% result differences) with the nonparallel theory of Hall *et al.* (1984) near both the upper and lower branches.

With a weakly nonlinear theory and computations based on Fourier-series, Hall & Malik (1986) discovered a region of subcritical instability growth, which is shown in figure 2 with the experiments of Pfenninger & Bacon (1969) and Poll (1979, 1980) and the neutral curve of Hall *et al.* (1984). Consistent with the Pfenninger & Bacon (1969) experiments, large-amplitude disturbances became unstable before the linear critical point (subcritical). Furthermore, near the lower branch of the neutral curve, Hall & Malik (1986) observed equilibrium states for large-amplitude disturbances. Both Jiménez *et al.* (1990) and Theofilis (1993*b*) did not find this region of subcritical growth with temporal direct numerical simulation codes. Jiménez *et al.* (1990) contended that this subcritical growth region did not exist. Contrary to the findings of Jiménez *et al.* (1990) and Theofilis (1993*b*), the nonlinear spatial direct numerical simulation results of Joslin (1994) showed both subcritical growth near the upper branch and nonlinear equilibrium states near the lower branch. These results are consistent with both the weakly nonlinear theory and the experimental results. It is clear from the results of Joslin (1994) that the input disturbance amplitude in the work of Theofilis (1993*b*) was too small to generate a subcritically growing disturbance and that a different flow-acceleration pressure gradient was used by Jiménez *et al.* (1990), resulting in a decaying mode instead of a subcritically growing mode.

Hall & Seddougui (1990) studied oblique waves and their interaction in attachment-line flow at the large Reynolds number limit. They note that close to the attachment line a small band of destabilized oblique modes appear, interact with the two-dimensional mode, and cause a breakdown of the two-dimensional mode. In addition, they note that oblique modes become less important away from the attachment line and that low-frequency modes become the dominant mechanism (i.e. stationary crossflow modes). More recently, Criminale, Jackson & Lasseigne (1994) have performed an analysis of three-dimensional inviscid stagnation-point flow by solving an initial-value problem. They show that unstable disturbances can be found for a flow expansion away from the stagnation point in one transverse direction and toward the stagnation point in the other transverse direction. They hypothesize that the three-dimensionality of the flow might overcome the stabilizing effects of viscosity, rendering the inviscid instability trends.

The two-dimensional theories of Hall et al. (1984) and Hall & Malik (1986) have demonstrated that nonparallel flow and nonlinear disturbances expand the conventional quasi-parallel neutral-curve region. These results have been confirmed by the two-dimensional spatial direct numerical simulations of Joslin (1994). However, the true physical flow involves three-dimensional disturbances that are imbedded in a three-dimensional boundary-layer flow. The relative growth or decay of three-dimensional linear and nonlinear disturbances must be understood to properly interpret the experimental results (some of which are shown in figure 2). Furthermore, the instability of the attachment-line flow to three-dimensional disturbances must be understood to formulate theories and implement devices to prevent instability growth.

The goal of the present study is to compute the evolution of three-dimensional instabilities in an attachment-line boundary-layer flow. A three-dimensional spatial direct numerical simulation approach is developed to study the instabilities. These simulations differ from previous computational studies because the present numerical formulation does not assume periodicity in the flow and does not limit the form of the disturbances. Specific regions in the parameter space are investigated with the direct numerical 'simulation to verify the nonparallel theory of Hall et al. (1984) for infinitesimal three-dimensional disturbances. Furthermore, the three-dimensional results are compared with the two-dimensional simulation results, and the effects of steady suction and blowing on the three-dimensional instability growth are evaluated. Disturbances are generated off (but near) the attachment line, and the disturbance evolutions are computed and compared with quasi-two-dimensional results.

## 2. Problem formulation

For the problem at hand, the velocities $\tilde{\boldsymbol{u}} = (\tilde{u}, \tilde{v}, \tilde{w})$ and the pressure $\tilde{p}$ are solutions of the incompressible, unsteady Navier–Stokes equations. The instantaneous velocities $\tilde{\boldsymbol{u}}$ and the pressure $\tilde{p}$ may be decomposed into base and disturbance components as

$$\tilde{\boldsymbol{u}}(x, t) = U(x) + u(x, t) \quad \text{and} \quad \tilde{p}(x, t) = P(x) + p(x, t) \tag{2.1}$$

where the base flow is given by the velocities $U = (U, V, W)$ and the pressure $P$, and the disturbance component is given by the velocities $\boldsymbol{u} = (u, v, w)$ and the pressure $p$. A Cartesian coordinate system $x = (x, y, z)$ is used in which $x$ is aligned with the attachment line, $y$ is wall normal, and $z$ corresponds to the direction of flow acceleration away from the attachment line.

Originally described by Hall et al. (1984), the base flow referred to as a swept Hiemenz flow is a similarity solution to the incompressible three-dimensional Navier-

Stokes equations. Shown in figure 1, the fluid comes straight down toward the wall; it turns away from the attachment line into the $\pm z$-directions to form a boundary layer. In the $x$-direction, the flow is uniform. In the absence of sweep, $U_o$ is equal to 0 and the flow reduces to the two-dimensional stagnation flow first described by Hiemenz (1911). A boundary-layer thickness is defined in the $(y,z)$-plane as $\delta = (\nu L/W_o)^{1/2}$; a Reynolds number, as $R = U_o \delta/\nu = 2.475 R_\theta$; and a transpiration constant, as $\kappa = V_o(L/\nu W_o)^{1/2}$, where $\kappa = 0$ for the zero-suction case, $U_o, V_o, W_o$ are velocity scales, and $L$ is the length scale in the flow-acceleration direction $z$. If the attachment line is assumed to be infinitely long, the velocities become functions of $z$ and $y$ only, and the similarity solution can be found.

The equations for the base flow were given by Hall *et al.* (1984). If the solutions of these equations are nondimensionalized with respect to the attachment-line velocity $U_o$, the boundary-layer thickness $\delta$, and the kinematic viscosity $\nu$, then the base flow is

$$U(Y) = \hat{U}(Y), \quad V(Y) = \frac{1}{R}\hat{V}(Y), \quad \text{and} \quad W(Y,Z) = \frac{Z}{R}\hat{W}(Y) \qquad (2.2)$$

where $\{X, Y, Z\} = \{x, y, z\}/\delta$ and the hats refer to similarity variables. Note that in the character of this similarity solution, $U$ and $V$ are uniform along the attachment line and $W$ grows linearly with distance from the attachment line.

As Arnal (1994) demonstrated, the velocity profiles represented by equation (2.2) on the attachment line have properties which are very similar to Blasius flat-plate flow (except Blasius flow is slightly less stable than attachment-line flow). Therefore, we should expect viscous travelling-wave instabilities which are comparable to what we find in flat-plate flow. Namely, the instability can be viewed as an instability of the vorticity distribution, where the slight displacement of the voriticity can alter the process of production, convection, and diffusion of vorticity, which may tend to alter more and more the process and lead eventually to turbulence. However, the process is not clear off of the attachment line. Unlike two-dimensional flow problems, the divergence of the velocity components in the potential flow can influence the velocity profile shape and corresponding stability properties of the flow.

For the disturbance portion of equation (2.1), the three-dimensional incompressible Navier–Stokes equations are solved in disturbance form as

$$\frac{\partial u}{\partial t} + (u \cdot \nabla)u + (U \cdot \nabla)u + (u \cdot \nabla)U = -\nabla p + \frac{1}{R}\nabla^2 u \qquad (2.3)$$

with the continuity equation and boundary conditions

$$u = 0 \quad \text{at} \quad Y = 0 \quad \text{and} \quad u \to 0 \quad \text{as} \quad Y \to \infty. \qquad (2.4)$$

Disturbances are forced by harmonic-source generators, which involve suction and blowing at the wall and are assumed to decay to zero in the far field. At the inflow, solutions of the base flow are imposed, and the buffer-domain technique is employed as the outflow condition.

## 3. Numerical methods of solution

In the attachment-line $(X)$ direction, fourth-order central finite differences are used for the pressure equation and sixth-order compact differences are used for the momentum equations in the interior of the computational domain. At the boundary and near-boundary nodes, fourth-order forward and backward differences are used. The discretization yields a pentadiagonal system for the finite-difference scheme and

a tridiagonal system for the compact-difference scheme. The approximations can be solved efficiently by appropriate backward and forward substitutions.

In both the wall-normal ($Y$) and flow-acceleration ($Z$) directions, Chebyshev series are used to approximate the disturbances at Gauss–Lobatto collocation points. A Chebyshev series is used in the wall-normal direction because it provides good resolution in the high-gradient regions near the boundaries. Furthermore, the use of as few grid points as possible results in significant computational cost savings. In particular, the use of the Chebyshev series allows an efficient pressure solver. Because this series and its associated spectral operators are defined on [-1, 1] and the physical problem of interest has a truncated domain $[0, y_{max}]$ and $[-z_{max}, z_{max}]$, transformations are employed. Furthermore, stretching functions are used to cluster the grid near both the wall and the attachment line. For further details on the properties and the use of spectral methods, refer to Canuto *et al.* (1988).

For time marching, a time-splitting procedure was used with implicit Crank–Nicolson differencing for normal diffusion terms; an explicit three-stage Runge–Kutta method by Williamson (1980) was used for the remaining terms. For details of the time-marching procedure, refer to Joslin, Streett & Chang (1992). The solution is determined on a staggered grid. The intermediate Runga–Kutta velocities are determined on Gauss–Lobatto points. The pressure is found by solving the Poisson equation on Gauss points and is then spectrally interpolated onto Gauss–Lobatto points. Then, the full Runga–Kutta stage velocities are obtained from Gauss–Lobatto points with the updated pressure. The above system is solved three consecutive times to obtain full time-step velocities.

To satisfy global mass conservation, an influence-matrix method is employed and is described in some detail by Streett & Hussaini (1991), Danabasoglu, Biringen, & Streett (1990, 1991), and Joslin *et al.* (1992, 1993). For boundary-layer flow, four Poisson–Dirichlet problems are solved for the discrete mode that corresponds to the zero eigenvalue of the system; single Poisson–Neumann problems are solved for all other modes.

To efficiently solve the resulting Poisson problem, the tensor-product method of Lynch *et al.* (1964) is used. The discretized form of the Poisson equation for the pressure is

$$(L_x \otimes I \otimes I + I \otimes L_y \otimes I + I \otimes I \otimes L_z)\, p = R \qquad (3.1)$$

where $p$ is the desired pressure solution; the right side of the equation $R$ results from the time-splitting procedure; $I$ is the identity matrix; $L_x$ is the attachment-line-directed central finite-difference operator; $L_y$ and $L_z$ are the wall-normal-directed and flow-acceleration-directed spectral operators; and $\otimes$ denotes a tensor product. By decomposing the operators $L_y$ and $L_z$ into their respective eigenvalues and eigenvectors, we find

$$L_y = Q\Lambda_y Q^{-1} \qquad \text{and} \qquad L_z = S\Lambda_z S^{-1} \qquad (3.2)$$

where $Q$ and $S$ are the eigenvectors of $L_y$ and $L_z$, $Q^{-1}$ and $S^{-1}$ are inverse matrices of $Q$ and $S$, and $\Lambda_y$ and $\Lambda_z$ are the eigenvalues of $L_y$ and $L_z$. The solution procedure reduces to the following sequence of operations to determine the pressure $p$:

$$\left.\begin{aligned}
p^* &= (I \otimes Q^{-1} \otimes S^{-1})R, \\
p^\dagger &= (L_x \otimes I \otimes I + I \otimes \Lambda_y \otimes I + I \otimes I \otimes \Lambda_z)^{-1}p^*, \\
p &= (I \otimes Q \otimes S)p^\dagger.
\end{aligned}\right\} \qquad (3.3)$$

Because the number of grid points in the attachment-line direction is typically an
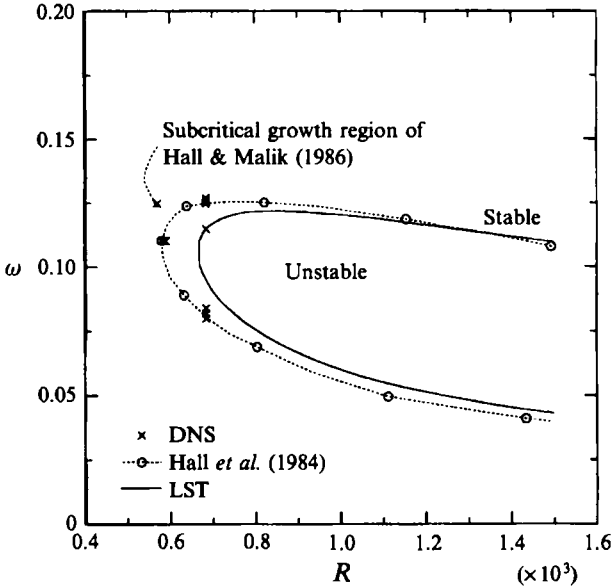
FIGURE 3. Neutral curves, region of subcritical instability growth, and sample points for direct numerical simulation in attachment-line boundary layer.

order of magnitude larger than the wall-normal and flow-acceleration directions, the operator $L_x$ is much larger than both $L_y$ and $L_z$. Because $L_x$ is large and has a sparse pentadiagonal structure and because $\Lambda_y$ and $\Lambda_z$ influence the diagonal only, an LU decomposition is performed for the second stage of equation (3.3) once, and forward and backward solutions are performed for each time step of the simulation. The first and third steps of the pressure solution for equation (3.3) involve matrix multiplications.

To obtain the attachment-line-directed operator $L_x$, central finite differences are used. To find the wall-normal $L_y$ and flow-acceleration $L_z$ operators, the following matrix operations are required:

$$L_y = I_{GL}^G D_y \tilde{D}_y I_G^{GL} \quad \text{and} \quad L_z = I_{GL}^G D_z \tilde{D}_z I_G^{GL} \tag{3.4}$$

where $D_y$ is a spectral wall-normal derivative operator for the stretched grid; $D_z$ is the spectral, derivative operator that is grid clustered in the attachment-line region; and $\tilde{D}_y$ and $\tilde{D}_z$ are the derivative operators with the first and last rows set to 0. The interpolation matrix $I_{GL}^G$ operates on variables at Gauss–Lobatto points and transforms them to Gauss points; the interpolation matrix $I_G^{GL}$ performs the inverse operation. The spectral operators are described in detail by Canuto *et al.* (1988) and Joslin *et al.* (1993).

The operators $\{L_x, L_y, L_z\}$, the eigenvalue matrices $\{\Lambda_y, \Lambda_z\}$, the eigenvector matrices $\{Q, Q^{-1}, S, S^{-1}\}$, and the influence matrix are all mesh-dependent matrices and must be calculated only once.

The buffer-domain technique introduced by Streett & Macaraeg (1989) is used for the outflow condition. As shown by Joslin *et al.* (1992) for the flat-plate boundary-layer problem, a buffer length of three disturbance wavelengths is adequate for travelling waves. The disturbances are assumed to be from the discrete spectrum, which exponentially decay with distance from the wall. Both at the wall and in the
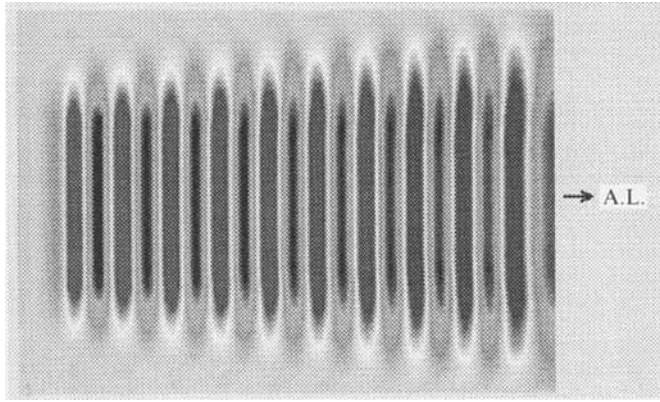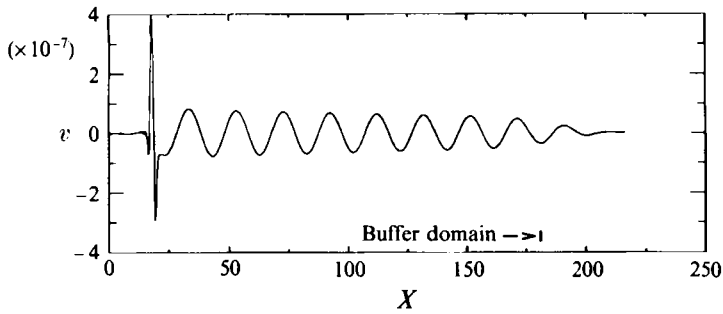
FIGURE 4. Side and top view of three-dimensional travelling wave
in attachment-line boundary layer.

far field, homogeneous Dirichlet conditions are imposed. Homogeneous Dirichlet and Neumann conditions have been used in the flow-accelerated direction. With either condition, the disturbance will develop in the same manner along the attachment line, provided that the boundaries are sufficiently far from the attachment-line region. The base flow is used for the inflow boundary condition.

Disturbances are forcibly imposed into the boundary layer by unsteady suction and blowing with the wall-normal velocity component through the wall (harmonic-source generators). An equal amount of mass injected by blowing is extracted by suction so that zero net mass is added to the boundary layer. A similar technique has been used by (among others) Danabasoglu, Biringen, & Streett (1991) in there study of periodic control by suction and blowing. Although the disturbances may be generated by random frequency input, the disturbances of interest here are forced with known frequencies. Essentially, this disturbance generator is an alteration to the no-slip boundary conditions which are conventionally used for the wall condition in a viscous flow problem.

## 4. Results

The spatial evolution of three-dimensional disturbances is computed by direct numerical simulation, which involves the solution to the unsteady, nonlinear, three-dimensional Navier–Stokes equations. The simulations are performed on a grid of 661 points ($\approx$ 60 points per wavelength) along the attachment line, 81 points in the wall-normal direction, and 25 points in the flow-acceleration direction. The far-
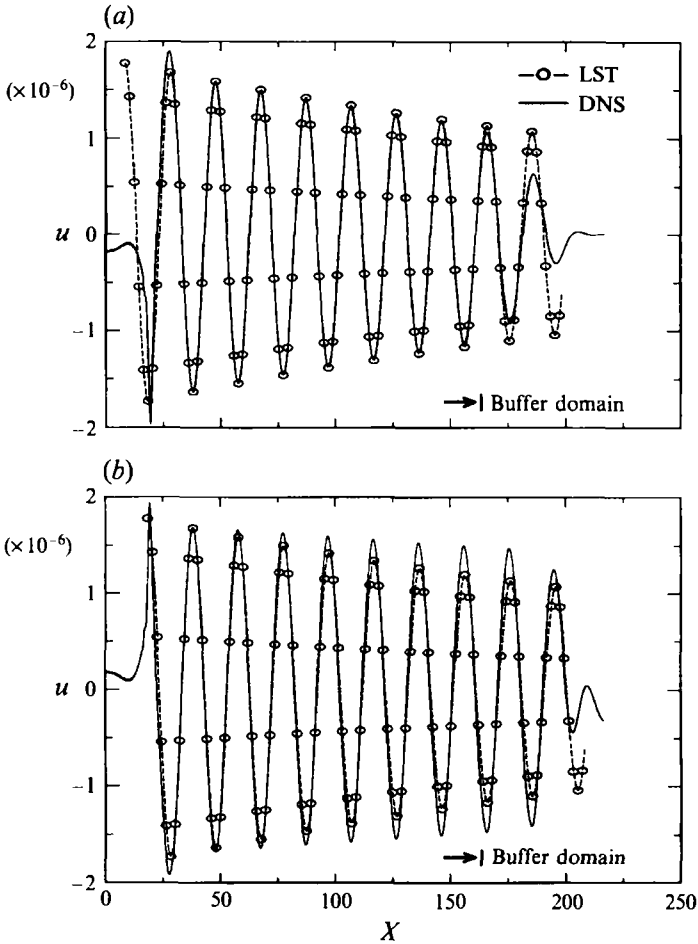
FIGURE 5. Simulated two-dimensional instability evolution (a) in parallel base-flow approximation ($V = 0$) and (b) in three-dimensional attachment-line base flow for $R = 570$ and $\omega = 0.1249$.

field boundary is located at $50\delta$ from the wall, the computational length along the attachment line is $216.56\delta$, and the flow-acceleration boundaries are located $\pm100\delta$ from the attachment line. For the time-marching scheme, the disturbance wavelength was divided into 320 time steps per period. The total Cray Y-MP time for a simulation with a single processor was approximately 25 hr. As shown in figure 3, the parameter regions of interest consist of a region of linear instability growth, a region of linear instability decay (which is the the region of nonlinear, subcritical instability growth identified by Hall & Malik 1986), the upper and lower branches of the neutral curve, and the critical region predicted by the nonparallel theory of Hall *et al.* 1984.

This study begins by validating the simulation results for infinitesimal disturbances with hydrodynamic stability theory with the special case of a frozen base flow. Nonparallel terms (i.e. the wall-normal base flow components) for the equations are included in the simulation and the instabilities are compared with the frozen-flow instability properties. Next, aspects of instability development on and near the attachment line are compared for quasi-two-dimensional and point-source harmonic-source generators with the theory of Hall *et al.* (1984). The effects of suction on the
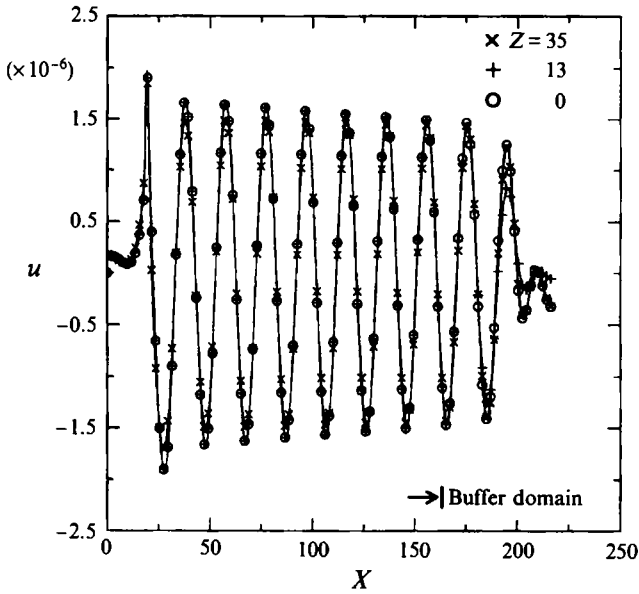
*R. D. Joslin*



FIGURE 6. Flow-acceleration variation of simulated two-dimensional instability evolution in three-dimensional attachment-line base flow for $R = 570$ and $\omega = 0.1249$.

### 4.1. *Region of disturbance decay*

The nonparallel theory of Hall *et al.* (1984) outlined the stable and unstable regions for infinitesimal disturbances. In a segment of the subcritical region, large-amplitude disturbances were found by Hall & Malik (1986) to exhibit nonlinear amplification. The two-dimensional spatial direct numerical simulation study by Joslin (1994) confirmed this subcritical growth phenomenon. In this section, the Reynolds number $R = 570$ and the frequency $\omega = 0.1249$, which are parameters in the subcritical region, are used in the study of the evolution of small-amplitude three-dimensional disturbances. The results are compared with linear stability theory and previous two-dimensional results.

To compare with the two-dimensional theory and previous simulations, a quasi-two-dimensional disturbance is initiated in the three-dimensional flow. At best, this disturbance is an approximation to a true two-dimensional instability mode. To generate this two-dimensional disturbance, a harmonic source is used that is elongated ($-44.2 < Z < 44.2$) in the flow-acceleration direction. This disturbance-forcing method is comparable to using a vibrating ribbon to generate two-dimensional disturbances for wind-tunnel experiments. The qualitative features of a disturbance generated by the harmonic source with a small amplitude (e.g. $A = 0.001\%$) are shown in figure 4. The disturbance evolution is viewed from above and along the attachment line. The wave travels along the attachment line without significant three-dimensional features. However, because the base flow is accelerating away from the attachment
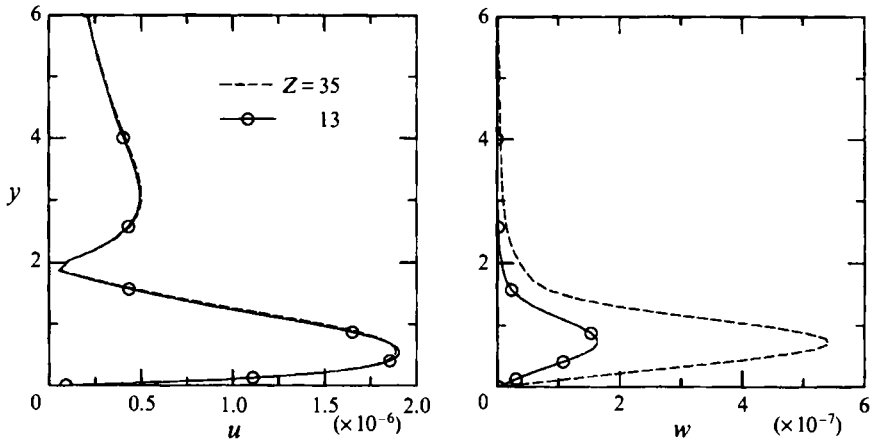
FIGURE 7. Comparison of three-dimensional disturbance velocity profiles at $X = 100$ near attachment line at $R = 570$ and $\omega = 0.1249$.

line (in the $\pm Z$-directions), wave spreading occurs with distance from the harmonic source, and the rate of spreading increases with distance along the attachment line.

Quasi-two-dimensional simulation results for both a quasi-parallel base flow (i.e. $V = 0$) and the full swept Hiemenz flow are compared with linear stability theory. The results are shown in figure 5. The amplitude, decay rate, and wavelength of disturbances simulated with the quasi-parallel flow are in very good quantitative agreement with the two-dimensional linear stability theory results. This agreement suggests that in this parameter region the elongated harmonic source can approximate a two-dimensional disturbance along the attachment line. Figure 5 also shows that the full swept Hiemenz base flow destabilizes disturbances due to the inclusion of the $V$ velocity component. This destabilizing feature is consistent with the results reported in the two-dimensional nonparallel studies by Hall *et al.* (1984) and Joslin (1994).

To further demonstrate the two-dimensional nature of the disturbance generated with the elongated harmonic source, figure 6 shows the attachment-line results compared with results at a distances $13\delta$ and $35\delta$ off the attachment line. The evolution patterns are identical out to near $35\delta$, where small deviations are observed. This implies that the elongated harmonic source is generating primarily two-dimensional waves and that the attachment-line velocity component is dominant (i.e. the amplitude of the $w$ velocity component of the disturbance is too small to modify the dominant $u$ component). Figure 7 shows $u$ and $w$ velocity profiles at $Z = 13\delta$ and $35\delta$. Although only small differences are found with $u$ velocity components, the $w$ velocity components are in strong disagreement. Note that the $w$ velocity is an order of magnitude smaller than the $u$ velocity, which is the reason for the good agreement between the $u$ velocity on the attachment line with the same components off the attachment line. Furthermore, although no symmetry assumption is made, flow symmetry about the attachment line is realized with this particular harmonic-source generator.

In figures 8 and 9, three-dimensional simulation results on the attachment line are compared with previous two-dimensional simulation results by Joslin (1994). Figure 8 clearly shows a significant amplitude disparity between the two- and three-dimensional results. Because the three-dimensional simulations contain a flow-acceleration veloc-
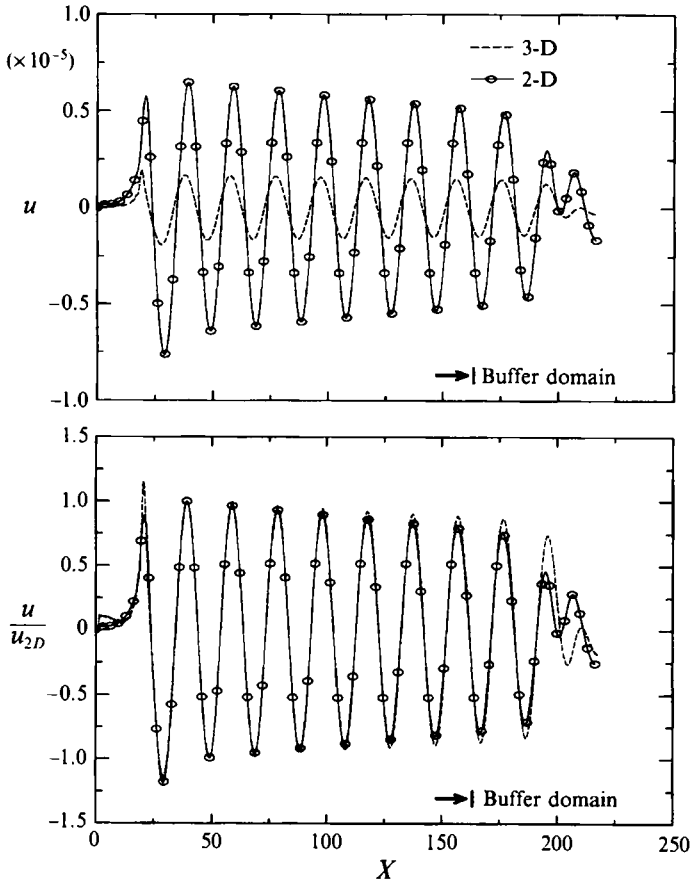
FIGURE 8. Comparison of two- and three-dimensional disturbance evolutions in three-dimensional attachment-line boundary layer for $R = 570$ and $\omega = 0.1249$.
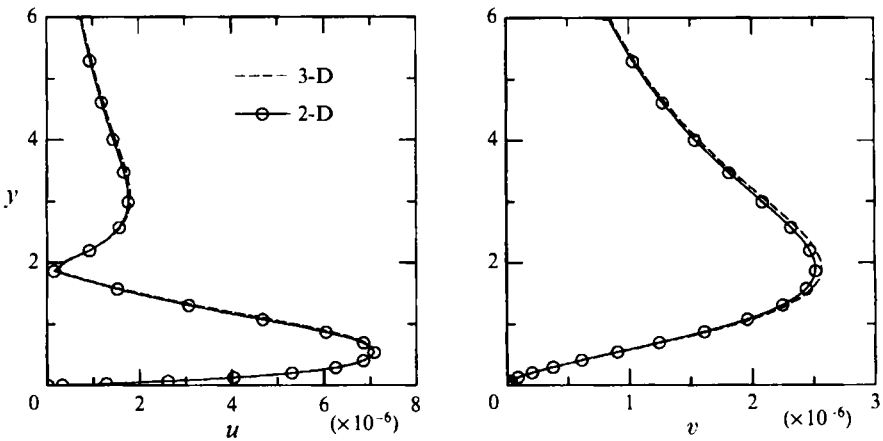


FIGURE 9. Comparison of normalized two- and three-dimensional disturbance velocity profiles at $X = 100$ in attachment-line boundary layer at $R = 570$ and $\omega = 0.1249$.
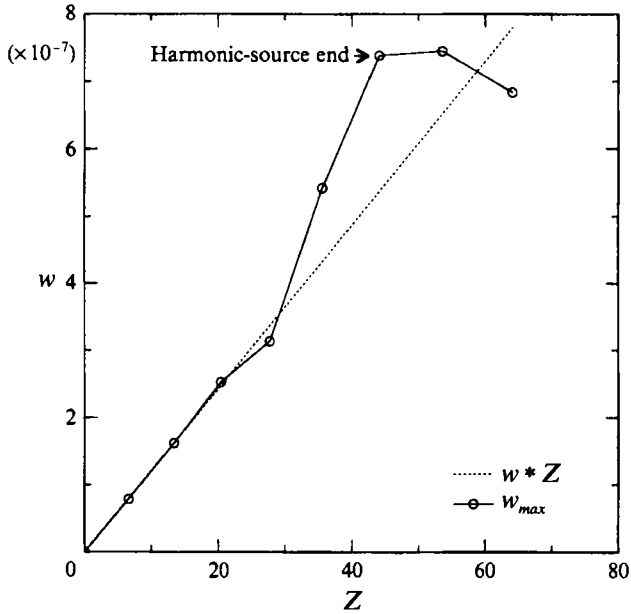
FIGURE 10. Maximum flow-accelerated disturbance velocity ($w$) with distance from attachment line at $X = 100$, $R = 570$, and $\omega = 0.1249$.

ity component ($w$), an additional degree of freedom is available to disperse (or absorb) energy. Hence, the harmonic-source generator forces less energy into the attachment-line velocity component ($u$). The two-dimensional and three-dimensional (normalized by the two-dimensional maximum of the $u$ velocity) results are also shown in figure 8 to enable a growth-rate comparison. The disturbance is slightly more destabilized in the full three-dimensional flow than in the two-dimensional flow approximation. Similar qualitative differences are evident when disturbance growth rates in quasi-parallel flow are compared with those in nonparallel flows. Finally, normalized disturbance velocity profiles are compared in figure 9. The shapes of the compared profiles agree well. The results demonstrate that two-dimensional simulations capture the qualitative features of the true three-dimensional flow; in addition, because a third degree of freedom ($w, z$) is not present in the two-dimensional simulations, amplitude information is overpredicted, and growth-rate information is underpredicted. These results suggest that much larger disturbances will be required to generate subcritical disturbance growth in the three-dimensional flow (if subcritical growth is possible for a single discrete mode in a three-dimensional flow).

In the nonparallel theory of Hall *et al.* (1984), the $z$-dependent form for the flow-accelerated velocity component ($w$) was a key assumption, which led to a system of ordinary differential equations, rather than partial differential equations. This assumed form is equivalent to the base-flow form: $W \rightarrow W_o Z$. Figure 10 shows the maximum amplitudes of the flow-accelerated velocity component at $X = 100$, away from the attachment line. For the present harmonic source, this $z$-dependent disturbance form assumed by Hall *et al.* (1984) is realized in the simulation near the attachment line; however, because the harmonic source has a finite length, the disturbance behaviour near the harmonic-source ends deviates from the expected $z$
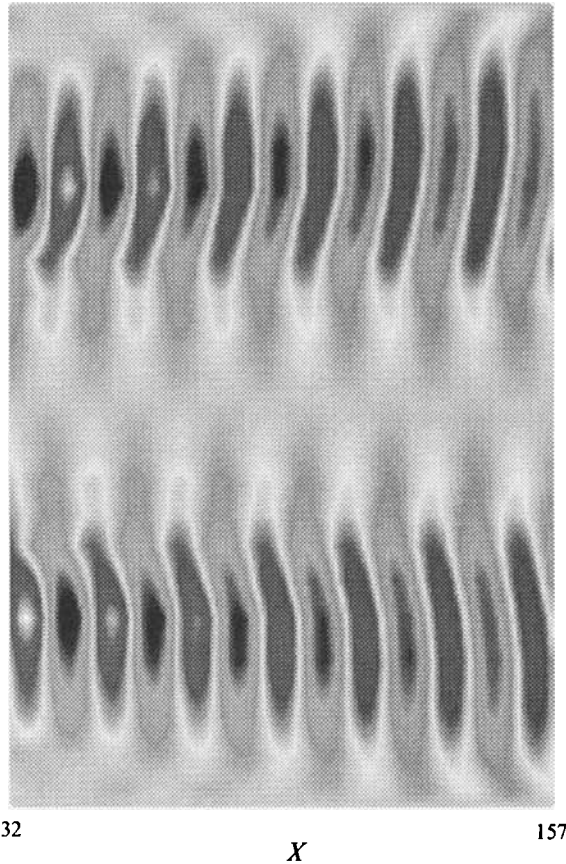
32                                                                              157
                                           *X*

FIGURE 11. Evolution of flow-accelerated disturbance velocity ($w$) in attachment-line boundary
layer at $R = 570$ and $\omega = 0.1249$. (Disturbance generated between $X = 16$ and 19.)

dependence. The harmonic-source ends cause a perturbation to the flow that is shown
both in figure 10 and in a top view of the flow in figure 11. Similar difficulties in
disturbance initialization can be found in the experiments; however, the core of the
test region (i.e. the attachment line) is not significantly contaminated by these end
effects.

### 4.2. *The neutral-curve region*

In parameter regimes near the neutral curve, finite Reynolds number disturbance
modes are studied near the upper branch, the lower branch, and the critical point.
Specifically, the simulations are conducted (in the regions shown in figure 3) to verify
the nonparallel theory of Hall *et al.* (1984).

For the upper branch, three simulations are performed to identify the neutral
curve. The harmonic-source disturbance generator is used to generate the quasi-two-
dimensional modes on the attachment line. For the Reynolds number $R = 684.2$, the
three-dimensional simulation results are shown in figure 12 for various frequencies.
The upper branch of the neutral curve is shown at the frequency $\omega = 0.1263$; the
nonparallel theory of Hall *et al.* (1984) and the two-dimensional simulations of Joslin
(1994) report that the upper branch is between $\omega = 0.1230$ and $\omega = 0.1240$. Although
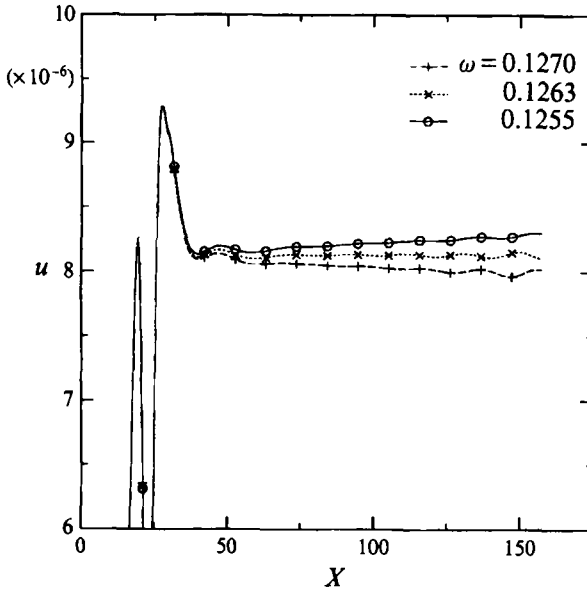the two- and three-dimensional results yield different upper branch locations, the

FIGURE 12. Instability growth and decay near branch II of curve of neutral stability for attachment-line boundary layer at $R = 684.2$.
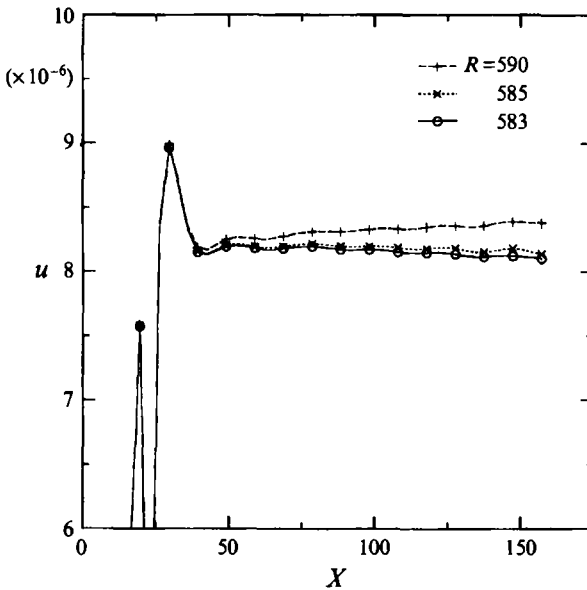


FIGURE 13. Instability growth and decay near critical point of curve of neutral stability for attachment-line boundary layer at $\omega = 0.1104$.

relative error, or difference, in the locations is only about 2%. This difference may be attributed to the assumption that a two-dimensional disturbance is generated from a three-dimensional harmonic source or that the three-dimensional base flow does not support pure two-dimensional disturbances.
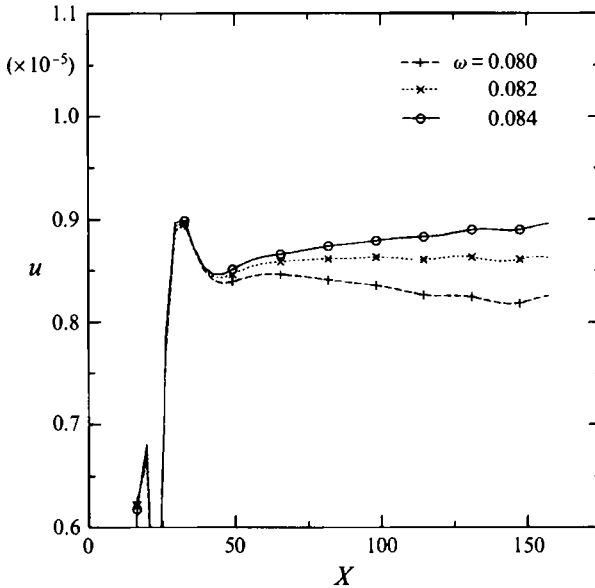
FIGURE 14. Instability growth and decay near branch I of curve of neutral stability for attachment-line boundary layer at $R = 684.2$.

Near the critical-point region of the neutral curve, computations are made to verify the critical point predicted by the nonparallel theory. Digitized data from the results of Hall et al. (1984) indicate that the Reynolds number $R = 580$ and frequency $\omega = 0.1104$ is the point furthest upstream at which an infinitesimal, two-dimensional disturbance becomes unstable. Although this value is not the exact critical point, this Reynolds number/frequency combination lies on the neutral curve in the region of the critical point. The computational results for disturbances in this critical-point region are shown in figure 13. The three-dimensional results suggest that for the frequency of $\omega = 0.1104$, the Reynolds number for neutral stability is slightly greater than $R = 585$. This leads to less than 1% difference between the nonparallel theory and the simulation results.

Finally, figure 14 shows results from simulations performed in the vicinity of the lower branch of the neutral curve. The results indicate that for the Reynolds number $R = 684.2$ the lower branch of the neutral curve is approximately at the frequency $\omega = 0.082$, which agrees with nonparallel theory.

For practical engineering purposes, the nonparallel theory of Hall et al. (1984) agrees with the three-dimensional simulation results in the limit of infinitesimal quasi-two-dimensional disturbances that propagate along the attachment line.

### 4.3. Three-dimensional disturbances

To generate three-dimensional disturbances, the flow-acceleration length of the harmonic-source generator is reduced to enable a more direct transfer of energy to the $w$ velocity component. Disturbances computed in the parameter regime described by a Reynolds number $R = 570$ and frequency $\omega = 0.1249$ are shown in figure 15. By reducing the length of the original harmonic source from $-44.2 < Z < 44.2$ to $-20.4 < Z < 20.4$, the generated disturbance is very similar to the previous quasi-two-dimensional disturbance. However, by reducing the harmonic-source length to
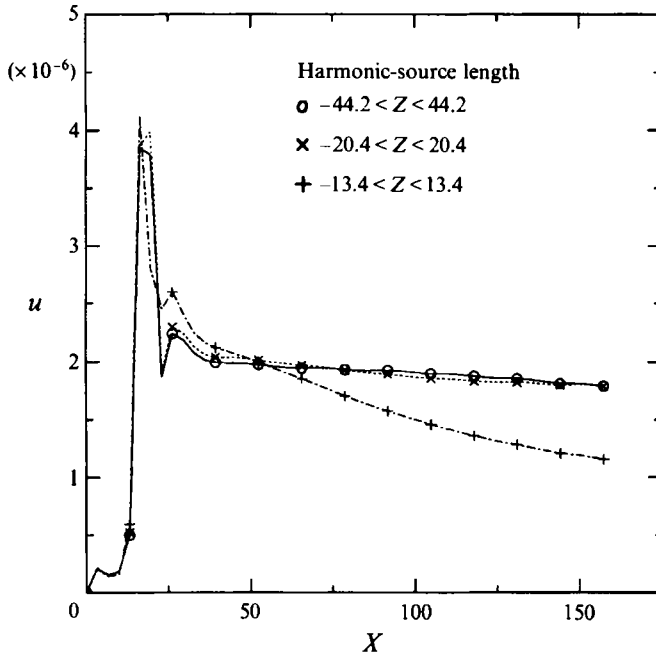
FIGURE 15. Evolution of disturbances in attachment-line boundary layer at $R = 570$ and $\omega = 0.1249$, where disturbances are generated with harmonic sources of various lengths.

$-13.4 < Z < 13.4$ (one-third of the original length), the generated disturbance is significantly stabilized on the attachment line. The evolution no longer represents a quasi-two-dimensional disturbance and becomes more comparable to a harmonic point source. Two-dimensional instabilities are apparently dominant on the attachment line.

Next, a harmonic-source generator is used to introduce a disturbance off the attachment line to determine the direction and rate of instability growth or decay. The results of a disturbance generated with a harmonic source located at $-27.8 < Z < 0$ are shown in figure 16. The top view indicates that the harmonic source generates a circular patterned disturbance that evolves along the attachment line with spreading both away from and toward the attachment line. These results suggest that the flow-accelerated shear away from the attachment line has insufficient strength to deter the spreading of the disturbance toward the attachment line. Figure 16 also shows that the maximum-amplitude $u$ velocity on the attachment line initially undergoes a slight decay and then continues to grow. The amplitude information along the attachment line suggests that an unstable mode is observed in the simulations; however, the top view of the flow field indicates that this amplification is caused by the wave spreading phenomenon. The combined amplitude and visual results imply that a disturbance generated off (but near) the attachment line can supply energy to the attachment region by the spreading of the wave pattern. In turn, this energy supply may feed an unstable mode on the attachment line.

For the final simulation in this section, the Reynolds number $R = 684.2$ and the frequency $\omega = 0.1150$ are used because the nonparallel theory predicts that infinitesimal two-dimensional disturbances are unstable on the attachment line. The disturbance is generated with a harmonic source which is positioned at $-35.6 <$
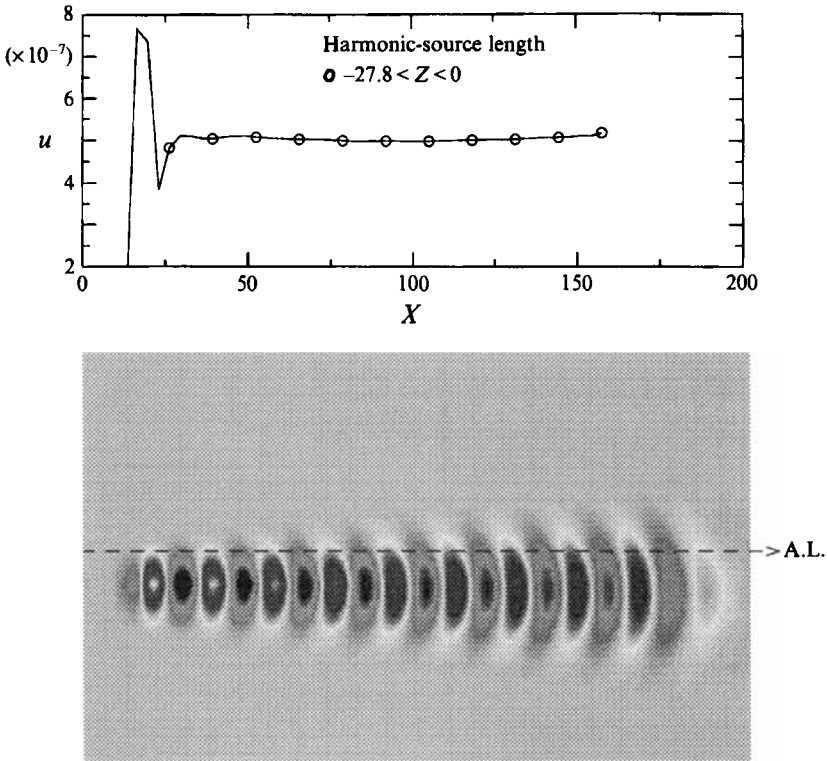
FIGURE 16. Evolution of disturbance velocity ($u$) on attachment line, and top view of three-dimensional travelling wave in attachment-line boundary layer at $R = 570$ and $\omega = 0.1249$.

$Z < -6.6$ (i.e. completely off the attachment line). The top view of the computed disturbance is shown in figure 17. The harmonic source has generated a disturbance with a circular pattern. As before, the disturbance evolves primarily along the attachment line, and the wave spreads both away from and toward the attachment line. Streamlines and vortex lines (determined by computing the trace of velocity and vorticity vectors) are overlaid on the disturbance pattern. These lines yield valuable information on the mean-flow-field properties near the attachment line. The disturbance packet follows the streamlines, and the packet spreads and evolves near the attachment line in a manner similar to packets in flat-plate boundary-layer flows. These results and the quasi-two-dimensional results suggest that the behaviour of instabilities in the region on and near the attachment line can be expected to be qualitatively similar to flat-plate boundary-layer instabilities. Supporting this postulation, the trace of velocity vectors in the wall-normal/flow-acceleration plane are shown at the top of figure 17. The resulting pattern in a reference frame moving with the disturbance velocity is reminiscent of Kelvin cat's eyes, which are observed in the two-dimensional flat-plate boundary-layer flow.

The amplitudes of the disturbance at various $Z$ locations are shown in figure 18. The disturbance has a peak amplitude initiated at $Z = -20.4$ and undergoes a strong decay along the attachment line, although the mode is predicted to be unstable on the attachment line. The spread of the disturbance toward the attachment line indicates that the disturbance on the attachment line is either unstable or merely gaining energy at a rate comparable to the spreading rate. However, because the
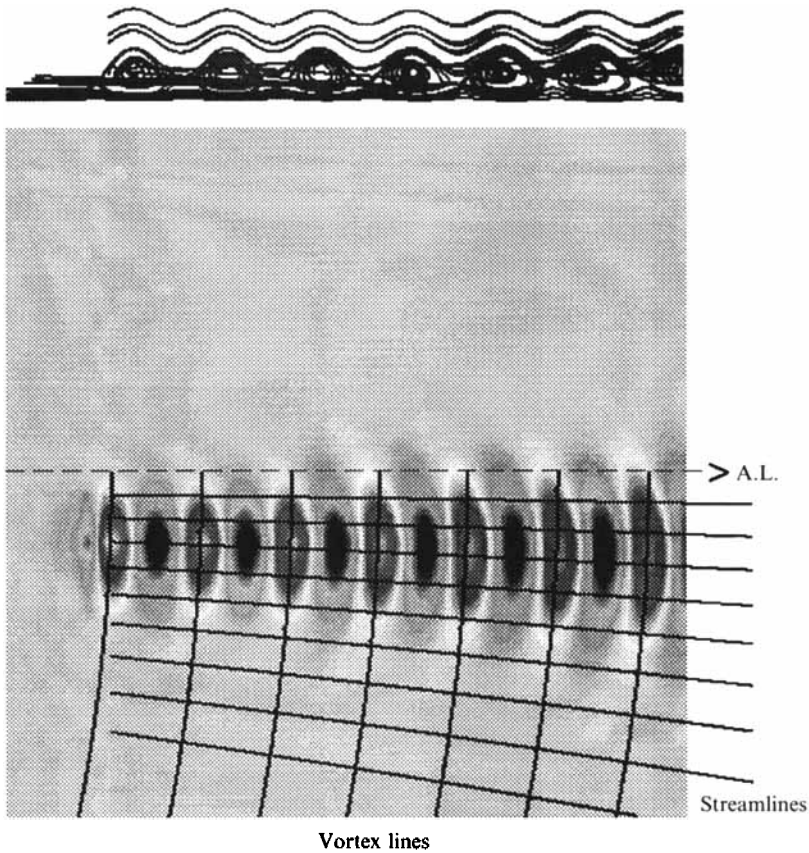
FIGURE 17. Top view of disturbance evolution in attachment-line boundary layer at $R = 684.2$ and $\omega = 0.1150$, where disturbance is generated with harmonic source near attachment line. The top part shows the trace of velocity vectors.

theory for two-dimensional disturbances indicates that the disturbance is unstable on the attachment line, some combination of energy transfer due to spreading and linear growth is likely. However, the more stable three-dimensional modes may rob the two-dimensional mode of enough energy to prevent flow transition along the attachment line. Note that the $u$ velocity components at all $Z$ locations indicate increased amplitudes along the attachment line, except for the $Z = -20.4$ location which indicates decay. Spreading causes the other $Z$ locations to receive energy, but because the $Z = -20.4$ location was the location of maximum initial amplitude and because the disturbance propagates along and away from the attachment line, the location of the maximum velocity is no longer at $Z = -20.4$. This results in an observed decay at the $Z = -20.4$ station. Figure 19 shows velocity profiles at various $Z$ locations at $X = 100$. As energy is transferred because of this spreading, the profiles near the attachment line undergo a distortion near the wall. This distortion leads to multiple maxima and profile shapes that deviate from the linear theory.

## 4.4. *Suction and blowing effects*

By changing the boundary conditions in the base equations from $\kappa = 0$, steady suction $(\kappa < 0)$ or blowing $(\kappa > 0)$ can be used to alter the growth or decay of disturbances
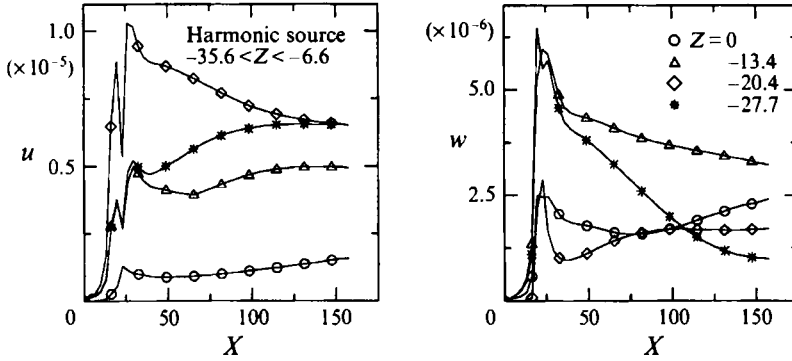
FIGURE 18. Evolution of disturbance generated off attachment line in attachment-line boundary layer at $R = 684.2$ and $\omega = 0.1150$.
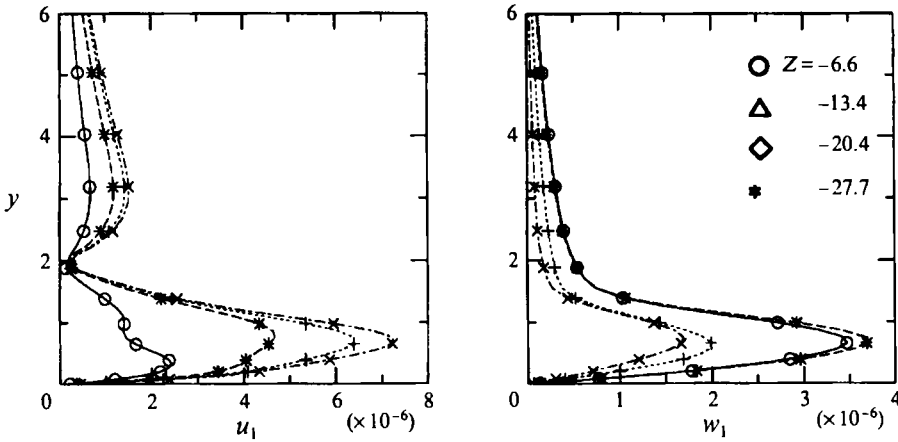


FIGURE 19. Comparison of three-dimensional disturbance velocity profiles at $X = 100$ near attachment line at $R = 684.2$ and $\omega = 0.1150$.

in the attachment-line boundary-layer flow. Near the upper branch of the neutral curve, the Reynolds number $R = 684.2$ and frequency $\omega = 0.1230$ are used for the simple test case of linear stability with suction and blowing. Shown in figure 20, the results of the quasi-two-dimensional disturbance generated with the elongated harmonic source ($-44.2 < Z < 44.2$) indicate that suction stabilizes the disturbance and blowing destabilizes the disturbance, which agrees with the theoretical results by Hall et al. (1984) and the two-dimensional simulation results by Joslin (1994).

The results for the three-dimensional disturbance generated with a harmonic source of length $-35.6 < Z < -6.6$ at the Reynolds number $R = 684.2$ and frequency $\omega = 0.1150$ indicated growth in the energy on the attachment line (figures 17–19). Because two-dimensional disturbances, which correspond to this Reynolds number and frequency, are linearly unstable on the attachment line, the presence of energy should lead to instability growth. Computations with suction are used to stabilize the disturbance on and near the attachment line. Clearly, figure 21 shows that suction stabilizes the disturbances located both on and off the attachment line.
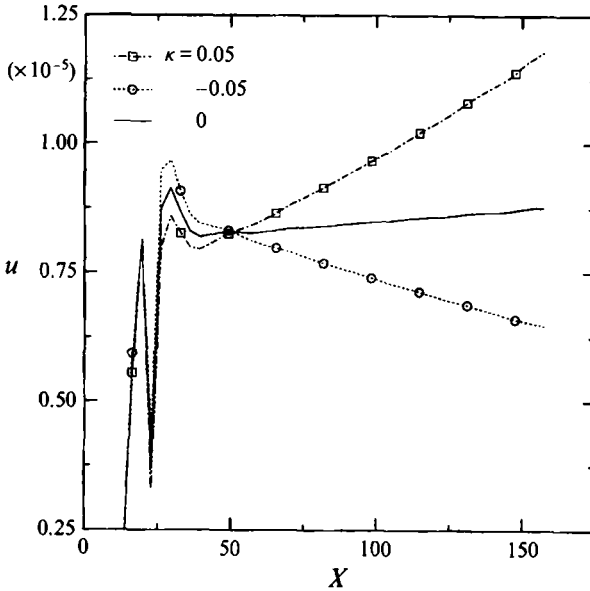
FIGURE 20. Effect of suction and blowing on growing instability modes in attachment-line boundary layer at $R = 684.2$ and $\omega = 0.1230$.
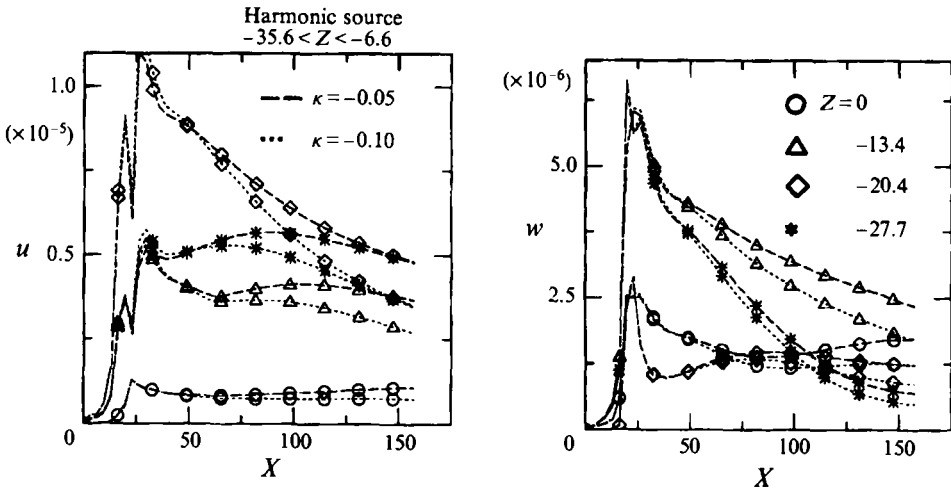


FIGURE 21. Effect of suction on evolution of disturbance generated off of attachment line in attachment-line boundary layer at $R = 684.2$ and $\omega = 0.1150$.

## 4.5. *Region of subcritical disturbance growth*

The weakly nonlinear theory and Fourier-based simulations by Hall & Malik (1986) reveal that a region of nonlinear subcritical growth exists for large-amplitude disturbances that evolve on the attachment line of a three-dimensional boundary-layer flow. The independent two-dimensional spatial direct numerical simulation study by Joslin (1994) confirmed this region of subcritical growth. Because the present results shown in figure 8 indicate that much larger harmonic-source amplitudes are required to initiate large-amplitude disturbances and because of the large computational costs

involved to resolve this nonlinear phenomenon, three-dimensional simulations of large-amplitude (potentially subcritical) instabilities will not be attempted in this paper.

## 5. Concluding remarks

In this paper, the results of three-dimensional spatial direct numerical simulations of attachment-line instabilities in swept Hiemenz flow are presented. A computational approach was described, which permits simulations of disturbances that evolve in flows where the periodic assumption is invalid.

Small-amplitude quasi-two-dimensional disturbances, computed in a quasi-parallel base flow, were shown to grow and decay in agreement with two-dimensional linear stability theory. For complete swept Hiemenz flow, disturbances are destabilized in comparison with those from both linear stability theory and two-dimensional simulation results.

The neutral-curve location predicted by the nonparallel theory of Hall *et al.* (1984) agreed well with the three-dimensional simulation results in the limit of infinitesimal quasi-two-dimensional disturbances, which propagate along the attachment line. Furthermore, the effects of both steady suction and blowing on small-amplitude disturbances were documented with direct numerical simulation. In agreement with the results of Hall *et al.* (1984), suction stabilizes small-amplitude disturbances, and blowing destabilizes these disturbances.

For the parameter regions studied here, instabilities that are generated from harmonic sources located off the attachment line spread both toward and away from the attachment line. Because of this spreading, energy from the initial disturbance is transferred to the attachment-line instabilities; however, suction stabilizes these instabilities. Disturbance packets generated near the attachment line follow the streamlines, and the packets spread and evolve near the attachment line in a manner similar to packets in flat-plate boundary-layer flows. Hence, instabilities in the region on and near the attachment line can be expected to be qualitatively similar to flat-plate boundary-layer instabilities.

Although the present study has demonstrated that instabilities generated off the attachment-line can spread and feed energy to attachment-line modes, the results do not indicate which modes receive this energy or whether these modes are unstable. A parameter study would provide this important information. Because of the significant computer resources required for the nonlinear three-dimensional Navier–Stokes computations, a parameter study could not be performed for the range of three-dimensional viscous instabilities. Such a study was recently conducted by Lin & Malik (1994). From the three-dimensional linear computations by Lin & Malik (1994), unstable instabilities in addition to the dominant two-dimensional wave were discovered by permitting nonuniformities in the flow-acceleration direction ($Z$). They showed that both asymmetric and symmetric modes, which have phase differences with distance from the attachment line, can be unstable depending on the Reynolds number. Although these new modes are linearly stable in the subcritical region outlined by Hall & Malik (1986), perhaps some combination of small (but finite)-amplitude modes may initiate a decline in the critical Reynolds number in a manner similar to the trend suggested by the nonlinear subcritical growth predicted by Hall & Malik (1986). Because Hall & Malik considered only the two-dimensional, uniform symmetric mode, very large amplitudes (12% of mean) were required to initiate this subcritical growth. With the discovery of these new

modes, the required amplitudes for subcritical growth may feasibly be generated by very small discontinuities (e.g. the accumulation of debris on the wing) across the attachment line. Further investigation of these nonuniform asymmetric modes should be pursued. A subsequent study by Lin and Joslin is currently underway to explore the nonlinear interaction of these nonuniform asymmetric and symmetric modes.

Swept Hiemenz flow serves as a very good model for studying transition mechanisms related to swept-winged transition because both travelling-wave instabilities along the attachment line may be studied and stationary and travelling crossflow-vortex instabilites can be studied in the flow-acceleration direction (over the wing chord). Such a study could potentially link a receptivity mechanism which causes waves along the attachment line with streamwise vorticity in the flow-acceleration direction.

## REFERENCES

ARNAL, D. 1994 Boundary layer transition: prediction, application to drag reduction. *AGARD FDP/VKI Course on Skin Friction Drag Reduction*, Brussels, Belgium/March 2-6, 1992.

CANUTO, C., HUSSAINI, M. Y., QUARTERONI, A. & ZANG, T. A. 1988 *Spectral Methods in Fluid Dynamics*. Springer.

CRIMINALE, W. O., JACKSON, T. L. & LASSEIGNE, D. G. 1994 Evolution of disturbances in stagnation-point flow. *J. Fluid Mech.* **270**, 331–347.

CUMPSTY, N. A. & HEAD, M. R. 1969 The calculation of the three-dimensional turbulent boundary layer. Part III: Comparison of attachment-line calculations with experiment. *Aero. Q.* **20**, 99–113.

DANABASOGLU, G., BIRINGEN, S. & STREETT, C. L. 1990 Numerical simulation of spatially-evolving instability control in plane channel flow. *AIAA Paper* 90–1530.

DANABASOGLU, G., BIRINGEN, S. & STREETT, C. L. 1991 Spatial simulation of instability control by periodic suction and blowing. *Phys. Fluids* A **3**, 2138–2147.

GASTER, M. 1965 A simple device for preventing turbulent contamination on swept leading edges. *J. R. Aero. Soc.* **69**, 788–789.

GASTER, M. 1967 On the flow along swept leading edges. *Aero. Q.* **18**, 165–184.

HALL, P. & MALIK, M. R. 1986 On the instability of a three-dimensional attachment-line boundary layer: weakly nonlinear theory and a numerical simulation. *J. Fluid Mech.* **163**, 257–282.

HALL, P., MALIK, M. R. & POLL, D. I. A. 1984 On the stability of an infinite swept attachment line boundary layer. *Proc. R. Soc. Lond.* A**395**, 229–245.

HALL, P. & SEDDOUGUI, S. O. 1990 Wave interactions in a three-dimensional attachment-line boundary layer. *J. Fluid Mech.* **217**, 367–390.

HIEMENZ, K. 1911 Die Grenzschicht an einem in den gleichförmigen Flüssigkeitsstrom eingetauchten geraden Kreiszylinder. Thesis, Göttingen. *Dingl. Polytechn. J.* **326**, 321.

JIMÉNEZ, J., MARTEL, C., AGÜÍ, J. C. & ZUFIRIA, J. A. 1990 Direct numerical simulation of transition in the incompressible leading edge boundary layer. *ETSIA/MF–903*.

JOSLIN, R. D. 1994 Direct numerical simulation of nonlinear instabilities in an attachment-line boundary layer. *Fluid Dyn. Res.* (submitted for publication).

JOSLIN, R. D., STREETT, C. L. & CHANG, C.-L. 1992 Validation of three-dimensional incompressible spatial direct numerical simulation code — A comparison with linear stability and parabolic stability equations theories for boundary-layer transition on a flat plate. *NASA TP*–3205.

JOSLIN, R. D., STREETT, C. L. & CHANG, C.-L. 1993 Spatial direct numerical simulation of boundary-layer transition mechanisms: Validation of PSE theory. *Theor. Comput. Fluid Dyn.* **4**, 271–288.

LYNCH, R. E., RICE, J. R. & THOMAS, D. H. 1964 Direct solution of partial difference equations by tensor product methods. *Numer. Maths.* **6**, 185–199.

PFENNINGER, W. 1977 Laminar flow control — Laminarization. *AGARD–R–654*.

PFENNINGER, W. & BACON, J. W. 1969 Amplified laminar boundary-layer oscillations and transition at the front attachment line of a 45 degree swept flat-nosed wing with and without boundary-layer suction. In *Viscous Drag Reduction* (ed. C. S. Wells), pp. 85–105. Plenum.

POLL, D. I. A. 1979 Transition in the infinite swept attachment line boundary layer. *Aero. Q.* **30**, 607–628.

POLL, D. I. A. 1980 Three-dimensional boundary layer transition via the mechanisms of attachment-line contamination and crossflow stability. In *Laminar-Turbulent Transition* (ed. R. Eppler & H. Fasel), pp. 253–262, Springer.

STREETT, C. L. & HUSSAINI, M. Y. 1991 A numerical simulation of the appearance of chaos in finite-length Taylor-Couette flow. *Appl. Numer. Maths* **7**, 41–71.

STREETT, C. L. & MACARAEG, M. G. 1989 Spectral multi-domain for large-scale fluid dynamic simulations. *Intl J. Appl. Numer. Maths* **6**, 123–140.

THEOFILIS, V. 1993a Numerical experiments on the stability of leading edge boundary layer flow: A two-dimensional linear study. *Intl J. Numer. Meth. Fluids* **16**, 153–170.

THEOFILIS, V. 1993b A spectral velocity-vorticity algorithm for the solution of the incompressible Navier–Stokes equations. In *Numerical Methods in Laminar-Turbulent Flow* (ed. C. Taylor), pp. 801–811. Pineridge

WILLIAMSON, J. H. 1980 Low-storage Runge-Kutta schemes. *J. Comput. Phys.* **35**, 48–56.